

# Cluster Counting Algorithm for Drift Chamber using LSTM and DGCNN\*

Zhe-Fei Tian,<sup>1</sup> Guang Zhao,<sup>2,†</sup> Ling-Hui Wu,<sup>2</sup> Zhen-Yu Zhang,<sup>1,‡</sup> Xiang Zhou,<sup>1</sup>  
Shui-Ting Xin,<sup>2</sup> Shuai-Yi Liu,<sup>2</sup> Gang Li,<sup>2</sup> Ming-Yi Dong,<sup>2,3</sup> and Sheng-Sen Sun<sup>2,3</sup>

<sup>1</sup>*Hubei Nuclear Solid Physics Key Laboratory, School of Physics and Technology, Wuhan University, Wuhan 430072, China*

<sup>2</sup>*Institute of High Energy Physics, Chinese Academy of Sciences, Beijing 100049, China*

<sup>3</sup>*University of Chinese Academy of Sciences, Beijing 100049, China*

Particle identification (PID) of hadrons plays a crucial role in particle physics experiments, especially for flavor physics and jet tagging. The cluster counting method, which measures the number of primary ionizations in gaseous detectors, represents a promising breakthrough in PID. However, developing an effective reconstruction algorithm for cluster counting remains a major challenge. In this study, we address this challenge by proposing a cluster counting algorithm based on long short-term memory and dynamic graph convolutional neural networks. Leveraging Monte Carlo simulated samples, our machine learning-based algorithm surpasses traditional methods. Specifically, it achieves a remarkable 10% improvement in  $K/\pi$  separation for PID performance.

Keywords: Particle identification, Cluster counting, Machine learning, Drift chamber

## I. INTRODUCTION

Particle identification (PID) of hadrons is crucial in high energy physics experiments, especially for flavor physics and jet tagging. Particle identification can help suppress combinatorial backgrounds, distinguish between the same topology final-states, and provide valuable additional information for flavor tagging of jets. Future particle physics experiments require advanced detector techniques with PID performance that surpasses the current generation.

The drift chamber is one of the key detectors in high energy physics experiments. In addition to charged particle tracking, the drift chamber can also provide excellent PID while requiring almost no additional detector budget. For a drift chamber, PID is based on the ionization behavior of charged particles traversing the working gas. A well-established technique to identify particles is the average ionization energy loss per unit length ( $dE/dx$ ) of charged particles measurement[1]. In a drift chamber cell, the charged particles ionize the gas, creating a cascade of electrons that can be detected as primary signals. This kind of ionization is called primary ionization, which is a Poisson process. Moreover, some of these electrons can also create secondary ionizations, leading to a Landau distributed  $dE/dx$ . The Landau distribution has an infinitely long tail and large fluctuations, limiting the  $dE/dx$  resolution[2]. Figure 1 shows an example of the waveform of the signal in a drift chamber cell.

---

\* Supported by Joint Fund of Research utilizing Large-Scale Scientific Facility of the NSFC and CAS under Contract No. U2032114, National Natural Science Foundation of China (NSFC) under Contract No. 12275296, Institute of High Energy Physics (Chinese Academy of Sciences) Innovative Project on Sciences and Technologies under Contracts Nos. E3545BU210 and E25456U210.

† Corresponding author, [zhaog@ihep.ac.cn](mailto:zhaog@ihep.ac.cn)

‡ Corresponding author, [zhenyuzhang@whu.edu.cn](mailto:zhenyuzhang@whu.edu.cn)

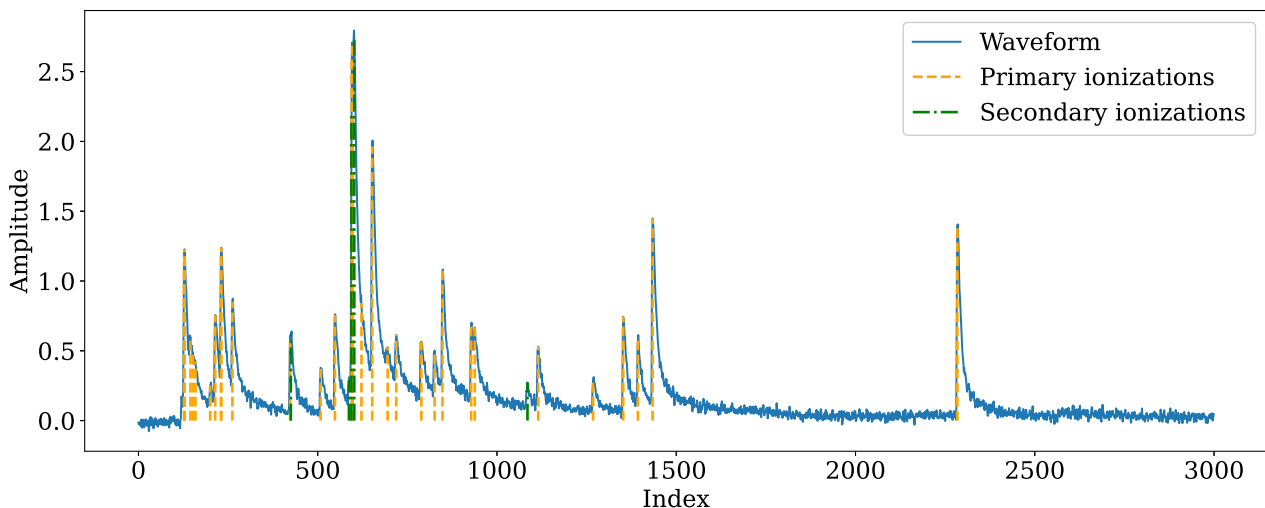


Fig. 1. A waveform example of induced current on a sense wire of drift chamber. Both primary and secondary ionizations contribute to the waveform. The orange lines indicate peaks from primary ionizations. The green lines indicate peaks from secondary ionizations.

Alternatively, the cluster counting technique directly measures the average number of primary ionizations per unit length in the waveforms processed by the fast electronics, rather than the  $dE/dx$ , which reduces the impact of the secondary ionizations[3] and significantly improves the PID performance. The resolution has the potential for a factor of 2 improvement for cluster counting. Therefore, cluster counting technique, which is the most promising breakthrough in PID, is proposed for the future colliders for the high-energy frontier, such as the Circular Electron-Positron Collider (CEPC)[4] and the Future Circular Collider (FCC)[5]. A previous study of the cluster counting for the BESIII upgrade demonstrates that the cluster counting method has exhibited superior PID performance compared to the  $dE/dx$  method. It significantly enhanced the PID performance for  $\pi/K$ , achieving about 1.7 times the separation power of the  $dE/dx$  method[6].

The stochastic nature of the ionization processes and the signal complexities present significant challenges in the development of an accurate and reliable cluster counting algorithm. In traditional methods, the cluster counting algorithm typically consists of two steps: derivative-based peak finding and time-based clusterization. For peak finding, the first and second derivatives are performed on the waveform, and signals are detected by threshold passing. However, the derivative-based algorithm is hard to achieve state-of-the-art for high pile-up and noise levels. For clusterization, as the average time differences for signals between clusters are larger than the ones for signals in the same cluster, one can exploit this information to design peak-merge algorithms. However, as the distributions of the time deference for the two cases are largely overlapped, the peak-merge algorithm suffers from low accuracy.

Machine learning (ML) is a rapidly growing field of computer science that involves the use of algorithms and statistical models to enable computer systems to improve their performance on a specific task by learning from data. Neural networks are the most commonly used ML technique at present, which are a set of computational models loosely inspired by the human brain consisting of an interconnected network. Recurrent neural networks (RNNs)[7] and graph neural networks (GNNs)[8] are both popular types of neural networks. In high energy physics, ML techniques are already applied in many experiments, such as ParticleNet based on GNN[9]. Machine learning has been preliminarily proved to be applicable in handling large-scale data in the field of high-energy physics. For cluster counting algorithm, ML can use full information of the waveform, and potentially uncover hidden features within the signal peaks. The problem can easily be modeled as a classification problem. Some mature ML tools can be applied, including PyTorch[10] and PyTorch Geometric[11].

In this paper, we present a ML algorithm to count the number of clusters in signal waveforms of drift chamber cells. This paper proceeds as follows: Sec. II introduces the fast simulation method and simulated samples used to train and test the ML algorithms. Sec. III introduces a new ML-based cluster counting algorithm. Sec. IV introduces the performance of the ML-based cluster counting algorithm and the comparison between it and traditional methods. Sec. V provides conclusions.

## II. SIMULATION AND DATA SETS

For the cluster counting study, a sophisticated first-principle simulation package was developed. The package simulates particle interactions and detector responses precisely, and creates realistic waveforms with MC truth timing as labels, which enables supervised training. The simulation package consists of two components: simulation and digitization. In the simulation, the geometry of drift chamber cells is constructed. Ionizations of charged particles are generated by the Heed package. To reduce

computational expense, the transportation, amplification and signal creation processes for each electron are parameterized according to the Garfield++ simulation results, which outputs analog waveforms for drift chamber cells[12]. In the digitization, data-driven electronics responses and noise is considered. The impulse response of the pre-amplifier is measured from the experiment and further convoluted with the waveform. The noise is extracted from the experimental data using the fast Fourier transform and added to the signal using the inverse fast Fourier transform. The digitization outputs realistic digitized waveforms, which exhibit good agreement with experimental data in terms of rise time of the peak and noise level. The flowchart of simulation is shown in Fig. 2.

The geometry in the simulation package is based on the design of the CEPC 4<sup>th</sup> conceptual detector, where the drift chamber has a cell size of  $1.8 \times 1.8 \text{ cm}^2$  and a gas mixture of He/iC<sub>4</sub>H<sub>10</sub>(90%/10%). According to the test beam experiments[13], the waveform roughly has a single-pulse risetime of 4 ns, a noise level of 5% and a sampling rate of 1.5 GHz. Based on the simulation package, MC samples with varying momenta are generated to train and test the neural networks. The detailed information of the samples is listed in Tab. 1.

Table 1. Summary of data sets used for training and testing ML-based cluster counting algorithms.

Purpose	Algorithm	Particle	Number of Events	Momentum (GeV/c)
Training	Peak finding	$\pi^\pm$	500,000	0.2 – 20.0
Testing	Peak finding	$\pi^\pm$	500,000	0.2 – 20.0
Training	Clusterization	$\pi^\pm$	500,000	0.2 – 20.0
Testing	Clusterization	$\pi^\pm$	$100,000 \times 7$	5.0/7.5/10.0/12.5/15.0/17.5/20.0
Testing	Clusterization	$K^\pm$	$100,000 \times 7$	5.0/7.5/10.0/12.5/15.0/17.5/20.0

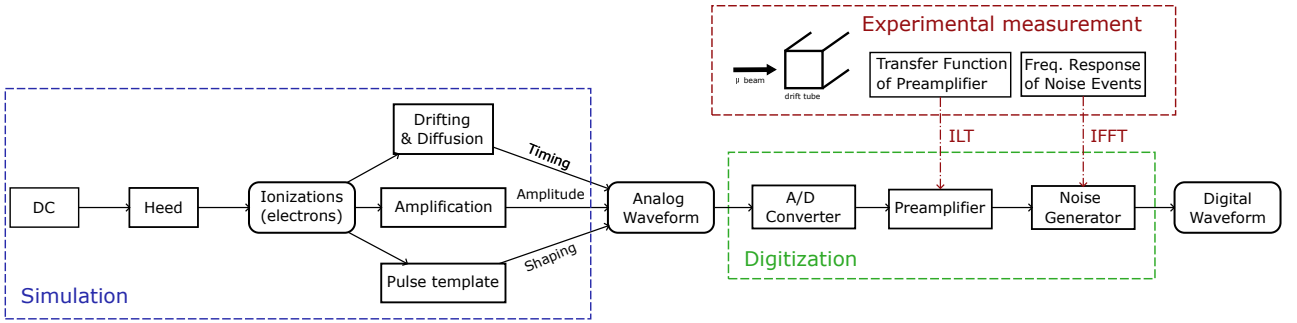


Fig. 2. Simulation package for cluster counting study. The package consists of simulation and digitization. The digitization takes input from the experimental experiments.

### III. METHODOLOGY

#### A. Algorithm Overview

The cluster counting reconstruction is performed through supervised learning on deep neural networks, using a large number of simulated labeled samples. As introduced in Sec. I, the cluster counting algorithm consists of two steps: peak finding and clusterization. In the first step, a long short-term memory (LSTM) network is employed to discriminate signals and noise. Both primary and secondary ionization signals are detected in this step. The second step of the algorithm, clusterization, is achieved through a dynamic graph neural network (DGCNN). The DGCNN is used to further classify whether a detected peak in the first step is from a primary ionization or not.

#### B. Peak finding

The peak finding algorithm is used to find all ionization peaks from a waveform. To reduce the complexity, the waveforms are divided into sliding windows with a window size of 15 data points. For each of these sliding windows, labels are added according to the MC truth information. The label can be either a signal candidate or a noise candidate, which defines the peak finding as a binary classification.

The LSTM is a type of RNN that can process sequential data and has been successfully used in a range of applications[14]. Its ability to model long-term dependencies in time series data makes it an ideal choice for the peak finding task because the slicing windows themselves are also time series data. A neural network based on the LSTM is used for peak finding, including the following layers:

- An LSTM layer

The LSTM layer is used for processing sequential data and capturing long-term dependencies between data points. This LSTM layer has one feature in the input data and 32 features in the hidden state.

- Two linear layers

The neural network model consists of two linear layers that serve as fully connected layers. The first layer has an input size of 32 and an output size of 32. The second layer has an input size of 32 and an output size of 1. A sigmoid activation function is applied to the output of the second layer to produce the final classification result.

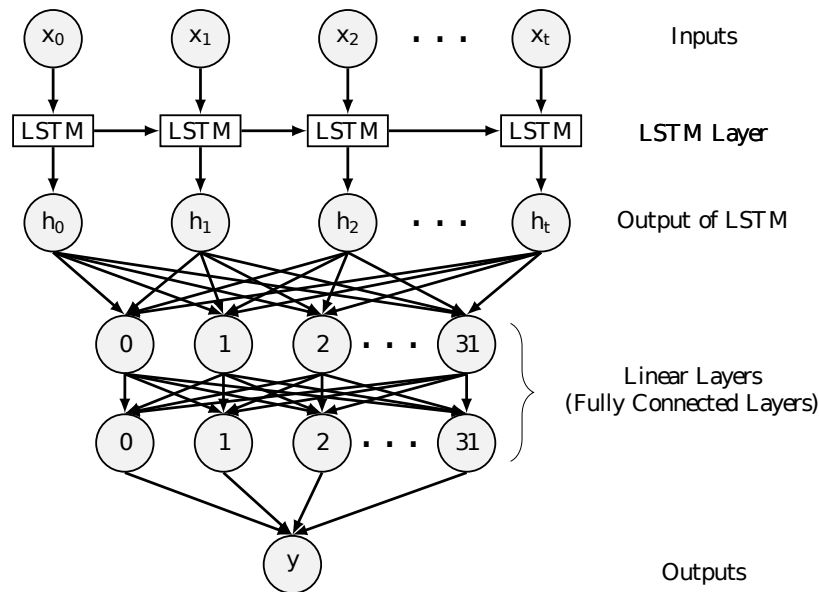


Fig. 3. The neural network structure of the LSTM-based model for the peak finding algorithm.

Figure 3 shows the network structure of the LSTM model used to train the peak finding algorithm. The model is trained on a simulated sample of  $\pi$  mesons. The sample includes  $5 \times 10^5$  waveform events with momenta ranging from  $0.2 \text{ GeV}/c$  to  $20 \text{ GeV}/c$ .

### C. Clusterization

After performing the LSTM-based peak finding algorithm, all the ionization signal peaks, including both primary and secondary ones, are detected. Therefore, a second algorithm, which is called clusterization algorithm, is developed to determine the number of primary ionization peaks.

In principle, secondary ionization occurs locally with respect to the primary electrons if the primary electrons have large enough energy. This leads to the electrons from a single cluster being located close to each other in the waveform. One can exploit this property to design an algorithm to discriminate primary and secondary electrons. As mentioned in Sec. I, the traditional algorithm is developed based on timing information in adjacent peaks. Graph neural network (GNN), which is operated on graph-structured data, can handle information with great complexity. The key design element of GNNs is the use of pairwise message passing, such that graph nodes iteratively update their representations by exchanging information with their neighbors. If the timing information of peaks is set as the node feature, and the edges are initially connected according to timing similarities, the GNN can effectively learn the complex timing structure of the primary and secondary electrons through message passing.

The DGCNN is a special type of GNN, which is applied to the clusterization algorithm. The DGCNN is designed to learn from the local structure of point clouds and can be used for high-level tasks such as classification and segmentation. The edge

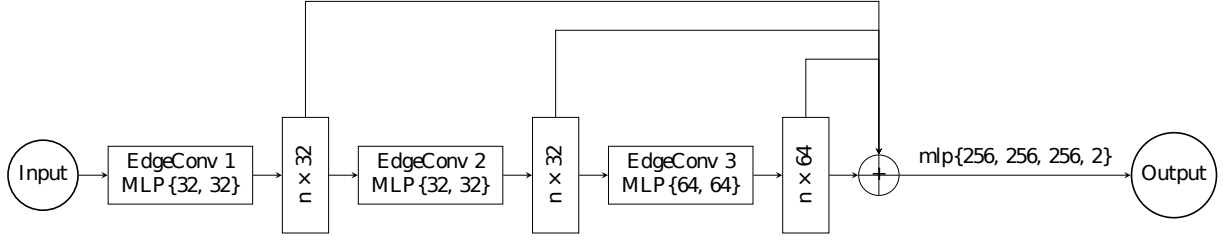


Fig. 4. The neural network structure of the DGCNN-based algorithm for clusterization.

convolution layer, which is the essential component of DGCNN, acts on graphs dynamically computed in each layer of the network. It is differentiable and can be plugged into existing architectures. In this work, the timings of the detected peaks in the peak finding are represented as a graph. The timing of individual peaks is represented as the node feature. The edge distance is defined as the timing similarity between nodes. The nodes are connected with the  $k^{\text{th}}$  nearest neighboring nodes. During the training, with message passing, the nodes update their features and update the connections[15]. Such a mechanism is expected to capture the hidden local relationships between peaks, thus achieving better performance in classifying primary and secondary ionizations. The clusterization algorithm network includes the following layers:

- Three dynamic edge convolution layers

Three dynamic edge convolution layers (DynamicEdgeConv) process graph-structured data by dynamically creating edges between each node and its neighboring nodes, thereby capturing local information. A new graph is generated at each layer of the GNN based on the  $k - \text{NN}$  approach. The MLP within the dynamic edge convolution layer maps the number of input channels to the number of output channels.

- A 4-layer multi-layer perceptron (MLP)

Multi-layer Perceptron (MLP) is a type of feedforward neural network that consists of multiple layers of neurons connected in a sequential manner[16]. This 4-layer MLP takes the concatenated output of the DynamicEdgeConv layers as input. It has 3 hidden layers each with 256 neurons and 1 output layer with 2 channels. It then passes this input through three fully connected layers, each with a 50% dropout rate. Finally, the model applies log softmax to the output of the MLP and returns the classification probabilities.

Figure 4 shows the neural network architecture of the clusterization. The model is trained by a pion sample with  $5 \times 10^5$  waveform events and momenta ranging from 0.2 GeV/c to 20 GeV/c.

#### IV. PERFORMANCE

The two-step model is trained using supervised learning on a large amount of waveform samples. To evaluate the generalization performance of the model, it is applied on testing samples.

For peak finding algorithm, both LSTM-based algorithm and traditional algorithm based on 2<sup>nd</sup>-derivative (D2) serve as classifiers. Their performance can be evaluated by the metrics of the classifier. In the context of classifiers, two commonly used metrics are precision and recall, which can also be referred to as purity and efficiency. The purity and efficiency are defined by true positive (TP), false positive (FP), and false negative (FN)[17], respectively. The specific definitions are provided in Eq. (1):

$$\begin{aligned} \text{Purity} &= \frac{\text{TP}}{\text{TP} + \text{FP}}, \\ \text{Efficiency} &= \frac{\text{TP}}{\text{TP} + \text{FN}}, \end{aligned} \quad (1)$$

where TP is the number of correctly detected peaks, (TP+FP) is the total number of detected peaks, and (TP+FN) is the total number of truth peaks in the waveform. The LSTM-based peak finding algorithm is tested on a  $\pi$  sample with momenta ranging from 0.2 GeV/c to 20.0 GeV/c. The sample consists of  $5 \times 10^5$  waveform events. For a classifier, the purity and efficiency values can be determined by applying varying probability thresholds. Figure 5 shows the purity and efficiency values of the LSTM-based peak finding algorithm and the traditional D2 algorithm as a function of the threshold. For the LSTM-based algorithm, a threshold of 0.95 is set, which gives a purity of 0.8986 and an efficiency of 0.8820. For the D2 algorithm, the threshold is set to have a similar purity to the LSTM-based algorithm, which gives an efficiency of 0.6827 (Tab. 2). Therefore, the LSTM-based algorithm is more efficient than the D2 algorithm, especially for the pile-up recovery (as shown in Fig. 6).

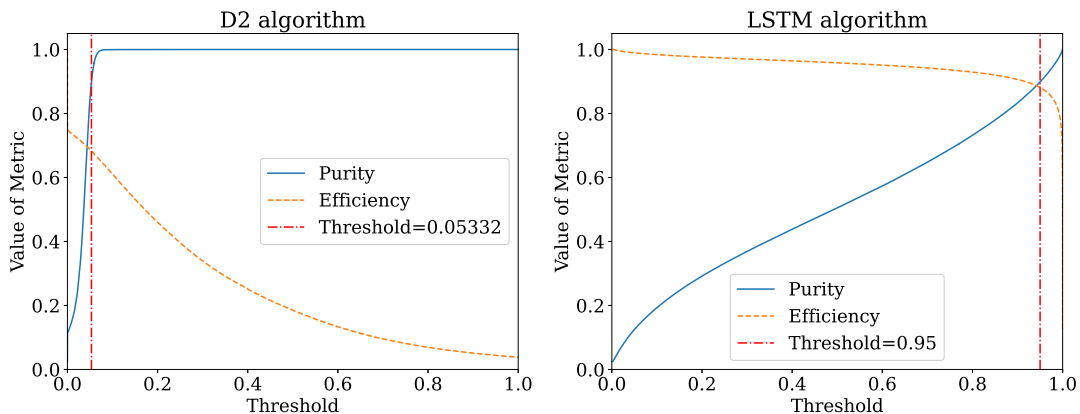


Fig. 5. Purity and efficiency as a function of the threshold for derivative-based D2 and LSTM-based algorithm, respectively. The blue solid line is the purity curve, the orange dashed line is the efficiency curve and the red dash dotted line is the optimized threshold.

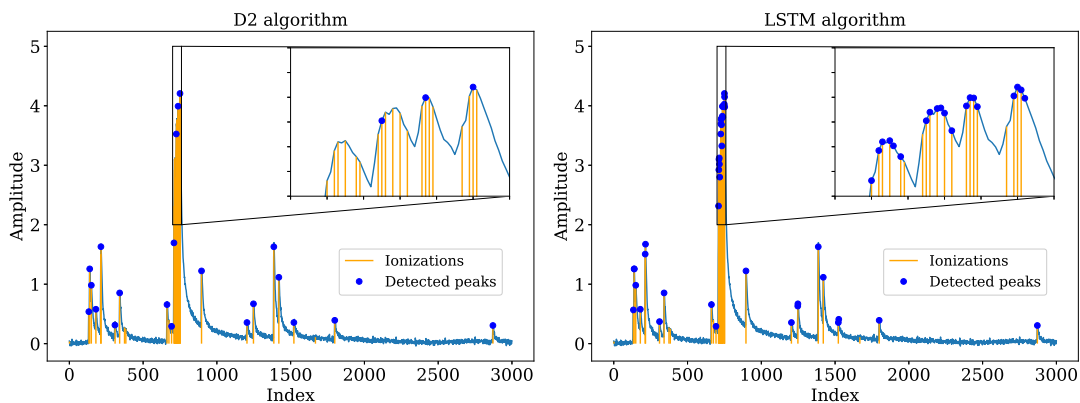


Fig. 6. Applying the derivative-based D2 and LSTM-based peak-finding algorithms on a simulated waveform. The blue points are the detected peaks. The orange lines are the peaks from the MC truth. The zoomed figure shows that the LSTM-based algorithm detects the pile-up peaks more accurately and more efficiently than the D2 algorithm.

Table 2. The purity and efficiency comparison between LSTM-based algorithm and traditional D2 algorithm for peak finding.

	Purity	Efficiency
LSTM algorithm	0.8986	0.8820
D2 algorithm	0.8986	0.6827

The clusterization algorithm is applied after the peak finding, aiming to determine the number of primary clusters from the detected peaks. After imposing both the LSTM-based peak finding and DGCNN-based clusterization algorithm, one can obtain the number-of-cluster distribution of a charged particle and calculate the separation power for particles in different species. In our study, the clusterization is completed by performing node classification in DGCNN. To achieve best performance, threshold of the classifier is optimized by requiring the best  $K/\pi$  separation power. The  $K/\pi$  separation power is defined as

$$S = \frac{\left| \left( \frac{dN}{dx} \right)_{\pi} - \left( \frac{dN}{dx} \right)_{K} \right|}{(\sigma_{\pi} + \sigma_K)/2}, \quad (2)$$

where  $dN/dx_{\pi(K)}$  and  $\sigma_{\pi(K)}$  are the measured value and measured error of the number of primary ionizations per length for  $\pi$  ( $K$ ). We perform the optimization using  $K/\pi$  samples with fixed momenta  $p = 5.0 \text{ GeV}/c, 7.5 \text{ GeV}/c, 10.0 \text{ GeV}/c, 12.5 \text{ GeV}/c, 15.0 \text{ GeV}/c, 17.5 \text{ GeV}/c,$  and  $20.0 \text{ GeV}/c$ , respectively. The solid blue, dashed violet and dashed cyan lines in Fig. 8 show the  $K/\pi$  separation power with different thresholds. According to the optimization, model with a threshold of 0.26 achieve overall best performance.

With the optimized threshold, Fig. 7 shows a comparison of the number-of-cluster distributions between the MC truth, the traditional algorithm and the DGCNN-based algorithm. It is shown that the number-of-cluster mean from the ML algorithm

is quite close to the MC truth and the relative resolution is better than the traditional algorithm. Figure 8 shows  $K/\pi$  separation powers of different algorithm at different momentum. The ML cluster counting algorithm achieves roughly 10% better separation power for all momenta range than the traditional algorithms. The detailed numeric results are listed in Tab. 3.

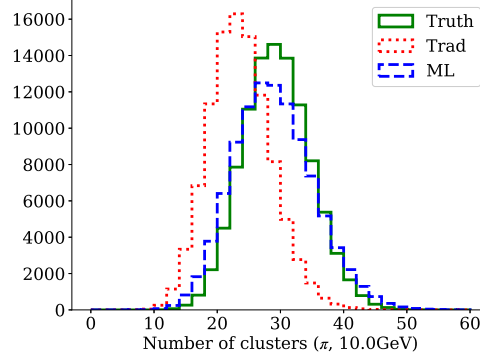


Fig. 7. The number of clusters distribution from MC truth (solid green), reconstruction by traditional algorithm (dotted red) and reconstruction by ML algorithm (dashed blue) for a 10 GeV/ $c$  pion sample, respectively.

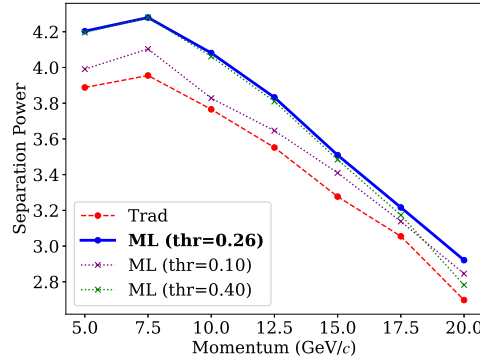


Fig. 8. The  $K/\pi$  separation power as a function of track momentum. The red dashed line is from the traditional algorithm, the blue solid, violet dotted and green dotted lines are from ML algorithm with a threshold of 0.26, 0.10 and 0.40, respectively. The blue solid line with a threshold of 0.26 achieves the overall best performance, which has a rough 10% better  $K/\pi$  separation than the traditional algorithm.

Table 3. Efficiency and separation power for charged  $K$  and  $\pi$  at various momenta and for different algorithms. The threshold of ML algorithm is optimized as 0.95 for LSTM-based peak finding algorithm and 0.26 for DGCNN-based clusterization algorithm. The efficiency is defined as the ratio of the number of reconstructed clusters to the number of MC truth clusters.

Algorithm	Metric	Momentum(GeV/ $c$ )							
		5.0	7.5	10.0	12.5	15.0	17.5	20.0	
ML algorithm	$\pi^\pm$ efficiency	1.003	1.001	0.999	0.999	0.998	0.998	0.999	
	$K^\pm$ efficiency	1.014	1.011	1.010	1.008	1.006	1.004	1.003	
	$K/\pi$ separation power	4.203	4.279	4.081	3.832	3.509	3.216	2.921	
Traditional algorithm	$\pi^\pm$ efficiency	0.814	0.808	0.803	0.801	0.801	0.800	0.800	
	$K^\pm$ efficiency	0.837	0.830	0.824	0.820	0.817	0.814	0.812	
	$K/\pi$ separation power	3.888	3.954	3.765	3.550	3.277	3.054	2.697	



## V. CONCLUSION

In this study, we have developed a cluster counting algorithm that incorporates both a peak-finding algorithm and a clusterization algorithm based on ML. Our approach offers several advantages over traditional methods for cluster counting. Specifically, our peak-finding algorithm demonstrates better efficiency compared to the derivative-based algorithm. The clusterization algorithm provides a Gaussian-distributed number of clusters and achieves an efficiency close to the ground truth (MC truth). The entire cluster counting algorithm outperforms the traditional methods, showcasing 10 % better  $K/\pi$  separation power. This level of PID performance with ML algorithms is roughly equivalent to having a 20% larger detector size with traditional algorithms. The critical role of ML algorithms in cluster counting suggests their potential application in future high-energy physics experiments.

**Data availability** The codes that support the findings of this study are openly available in github at [https://github.com/ZhefeiTian/cluster\\_counting\\_ml\\_codes](https://github.com/ZhefeiTian/cluster_counting_ml_codes).

- 
- [1] G. Charpak, R. Bouclier, T. Bressani et al., The use of multiwire proportional counters to select and localize charged particles. *Nucl. Instr. and Meth.* **62**, 262-268 (1968) doi: [10.1016/0029-554X\(68\)90371-6](https://doi.org/10.1016/0029-554X(68)90371-6).
  - [2] W. Blum, W. Riegler, L. Rolandi, Particle Detection with Drift Chambers. (2008) doi: [10.1007/978-3-540-76684-1](https://doi.org/10.1007/978-3-540-76684-1).
  - [3] A. H. Walenta, The Time Expansion Chamber and Single Ionization Cluster Measurement. *IEEE Trans. Nucl. Sci.* **26**, 73-80 (1979) doi: [10.1109/TNS.1979.4329616](https://doi.org/10.1109/TNS.1979.4329616).
  - [4] The CEPC Study Group, CEPC conceptual design report: volume 2 - physics & detector. (2018) doi: [10.48550/arXiv.1811.10545](https://doi.org/10.48550/arXiv.1811.10545).
  - [5] A. Abada, M. Abbrescia, S.S. AbdusSalam et al., FCC-ee: The Lepton Collider. *Eur. Phys. J. Spec. Top.* **228**, 261–623 (2019) doi: [10.1140/epjst/e2019-900045-4](https://doi.org/10.1140/epjst/e2019-900045-4).
  - [6] S.T. Xin, G. Zhao, L.H. Wu et al., Simulation study of particle identification using cluster counting technique for the BESIII drift chamber. *J. Instrum.* **18**, T01006 (2023) doi: [10.1088/1748-0221/18/01/T01006](https://doi.org/10.1088/1748-0221/18/01/T01006).
  - [7] A. Sherstinsky, Fundamentals of recurrent neural network (RNN) and long short-term Memory (LSTM) network. *Phys. D: Nonlinear Phenom.* **404**, 132306 (2020) doi: [10.1016/j.physd.2019.132306](https://doi.org/10.1016/j.physd.2019.132306)
  - [8] J. Zhou, G. Cui, S.D. Hu et al., Graph neural networks: A review of methods and applications. *AI Open* **1**, 57-81 (2020) doi: [10.1016/j.aiopen.2021.01.001](https://doi.org/10.1016/j.aiopen.2021.01.001).
  - [9] H.L. Qu, L. Gouskos, Jet tagging via particle clouds. *Phys. Rev. D* **101**, 056019 (2020) doi: [10.1103/PhysRevD.101.056019](https://doi.org/10.1103/PhysRevD.101.056019).
  - [10] A. Paszke, S. Gross, F. Massa et al., PyTorch: An Imperative Style, High-Performance Deep Learning Library. *Adv. Neural Inf. Process Syst.* **32**, 8024-8035 (2019) doi: [10.48550/arXiv.1912.01703](https://doi.org/10.48550/arXiv.1912.01703).
  - [11] M. Fey, J.E. Lenssen, Fast graph representation learning with PyTorch Geometric. *ICLR Workshop on Representation Learning on Graphs and Manifolds* (2019) doi: [10.48550/arXiv.1903.02428](https://doi.org/10.48550/arXiv.1903.02428).
  - [12] D. Pfeiffer, L. De Keukeleere, C. Azevedo et al., Interfacing Geant4, Garfield++ and Degrad for the simulation of gaseous detectors. *Nucl. Instr. and Meth. A* **935**, 121-134 (2019) doi: [10.1016/j.nima.2019.04.110](https://doi.org/10.1016/j.nima.2019.04.110).
  - [13] C. Caputo, G. Chiarello, A. Corvaglia et al., Particle identification with the cluster counting technique for the IDEA drift chamber. *Nucl. Instr. and Meth. A* **1048**, 167969 (2023) doi: [10.1016/j.nima.2022.167969](https://doi.org/10.1016/j.nima.2022.167969).
  - [14] S. Hochreiter, J. Schmidhuber, Long short-term memory. *Neural Comput.* **9**, 1735-1780 (1997) doi: [10.1162/neco.1997.9.8.1735](https://doi.org/10.1162/neco.1997.9.8.1735).
  - [15] Y. Wang, Y.B. Sun, Z.W. Liu et al., Dynamic graph CNN for learning on point clouds. *ACM Trans. Graph.* **38**, (2019) doi: [10.1145/3326362](https://doi.org/10.1145/3326362).
  - [16] A. Pinkus et al., Approximation theory of the MLP model in neural networks. *Acta Numer.* **8**, 143–195 (1999) doi: [10.1017/S0962492900002919](https://doi.org/10.1017/S0962492900002919).
  - [17] M. Hossin, M. N. Sulaiman, A review on evaluation metrics for data classification evaluations. *Int. J. Data Min. Knowl. Manag. Process* **5**, 1 (2015) doi: [10.5121/ijdkp.2015.5201](https://doi.org/10.5121/ijdkp.2015.5201).